ENHANCING SOLAR COLLECTOR PERFORMANCE: AN EXPERIMENTAL STUDY ON ZIGZAG RECTANGULAR ANGLED STRIPS AND NANOFLUID INTEGRATION

TAMIZHSELVAN LAKSHMANAN SELVAMANI [a*], SRIDHARAN VEERAPURAM [b]

[a*] Department of Mechanical Engineering , Rajalakshmi Engineering College , Thandalam, Tamil Nadu, India.

[b] Department of Mechanical Engineering , Sri Venkateswara College of Engineering , Pennalur, Sriperumbudur, Tamil Nadu, India.

[*] Corresponding author, E-mail: tamizhiisha@yahoo.com

Solar thermal collectors have become an increasingly popular technology for harnessing renewable energy and have gained significant attention as a sustainable solution to meet the growing global energy demands. These systems efficiently convert solar radiation into thermal energy, making them a viable option for a variety of applications across the residential, commercial, and industrial sectors. The use of nanofluids as the working fluid in solar thermal collectors has been extensively investigated as the incorporation of nanoparticles has been demonstrated to enhance the thermal properties of these systems ultimately leading to improvements in their overall efficiency. This experimental study investigates the performance of a conjugate flat-plate solar collector with the inclusion of zigzag rectangular shaped angled strips inside the absorber tube. The study also explores the use of various nanofluids such as MgO/DIW, ZnO/DIW, and Al_2O_3/DIW at a 1.0% volume concentration as the working fluid to determine their potential for enhancing the thermal efficiency of the solar collector. The experiments were conducted with 45^0 angled strips at three different pitch ratios (Y = 2.0, 3.0, and 4.0) under identical working conditions. The performance of the rectangular shaped zigzag strip enhanced collectors was systematically compared to that of plain conjugate flat-plate solar collector collectors. For a pitch ratio of 2.0, MgO/DIW, ZnO/DIW, and Al2O3/DIW improve heat transfer by 30%, 28%, and 22% at higher Reynolds numbers compared to DIW. The MgO/DIW consistently provides the highest heat transfer enhancement across all configurations and pitch ratios. The Nusselt number increases by 45%, 42%, and 40% for MgO/DIW, ZnO/DIW and Al2O3/DIW at a pitch ratio of 2.0 showed a significant enhancement in heat transfer due to nanoparticle effects and zigzag rectangular angled strip induced turbulence. The thermal efficiency reaches around 85% for MgO/DIW nanofluids compared to DIW at a lower pitch ratio of 2.0. The friction factor increases by 15% for ZnO/DIW at lower Reynolds numbers compared to DIW. The Pumping power increased by 10% for ZnO/DIW in zigzag rectangular angled strip tubes compared to plain tubes. These findings revealed that utilizing high thermal conductivity nanofluids and zigzag rectangular strip geometries with optimized pitch ratios can enhance the performance of heat transfer systems especially in applications such as solar energy collectors and heat exchangers.

Keywords: Conjugate Flat plate solar collector, Nanofluids, Zig Zag rectangular strip, thermal performance factor, friction factor ratio, Nusselt number ratio

1. Introduction

Solar thermal collectors are a crucial technology in the quest for renewable energy sources, as they efficiently convert solar radiation into useful thermal energy [1]. These systems have gained widespread interest due to their potential to address the growing global energy demands in a sustainable manner. In recent years, the incorporation of nanofluids as the working fluid in solar thermal collectors has been extensively investigated, as the addition of nanoparticles has been shown to enhance the thermal properties of these systems, ultimately leading to improvements in their overall efficiency [2]. Nanofluids are heterogeneous mixtures of a base fluid and nanoparticles that have garnered significant attention for their potential applications in various industries, including solar thermal systems [3]. Nanofluids exhibit enhanced thermal properties, such as increased thermal conductivity, compared to their base fluids, making them attractive for heat transfer applications. Yang et al. [4] explored the use of nanofluids as working fluids in solar thermal systems due to their enhanced thermal properties, yet concerns remain about nanoparticle agglomeration under cyclic heating. The result showed the thermal stability of oil-based CuO nanofluids highlighting the challenges of maintaining reliability in solar thermal applications. Hai et al. [5] numerically evaluated the energy and economic performance of a flat-plate solar collector (FPSC) using various nanofluids, including CuO-DW, Cu-DW, and hybrid nanocomposites, across different shapes and volume fractions. The results showed that CuO-Platelets at 1 vol.% and Re of 1900 achieved the highest thermal enhancement and reduced the solar collector size by 25.60%,CuO-Cylindrical and Cu-Platelets offered the lowest total cost of operation. Hawwash et al.[6] investigated the thermal performance of flat plate solar collectors (FPSC) using alumina oxide-water and copper oxide-water nanofluids, focusing on the effects of nanoparticle volume fraction and type. Their results revealed that a 0.5% volume fraction of copper oxide nanofluids achieved the highest thermal efficiency, achieving superior performance compared to alumina oxide-water nanofluids, despite the increased pressure drop in the collector. Mostafizur et al.[7] evaluated the performance of hybrid nanofluids in flat plate solar collectors focusing on parameters like entropy generation, exergy efficiency, and heat transfer. The results showed that CuO-MWCNT/water nanofluid reduced entropy generation and exhibited higher exergy efficiency compared to other nanofluids. The CuO-MWCNT/methanol nanofluid exhibited superior heat transfer properties but with increased entropy and lower exergy efficiency. Sheikholeslami et al.[8] conducted empirical and numerical studies to analyze the impact of nanofluids on heat transfer rates and overall efficiency. The review explored advancements in flat plate solar collectors, focusing on the integration of photovoltaic modules and the use of nanofluids to enhance thermal performance. Abhay et al. [9] evaluated the performance of a rectangular minichannel FPSC using Cu-water and TiO_2-water nanofluids. Cu-water nanofluids generally outperform TiO_2-water nanofluids in terms of fluid outlet temperature and mean plate temperature, while TiO_2-water nanofluids exhibit higher efficiency and heat removal factor. Saffarian et al [10]investigated the impact of flow direction and nanofluid type on heat transfer in a flat plate solar collector. The findings demonstrate that wavy pipes and CuO/water nanofluids can significantly enhance heat transfer coefficient across the acceptable pressure drop. Peng et al [11] numerically investigates the performance of a U-shaped evacuated tube solar collector using various oxide nanofluids. The results demonstrate that increasing the tube length and diameter using nanofluids, significantly enhance the thermal efficiency of collector . CuO nanofluids exhibit the highest performance improvement compared to other nanofluids and pure water. Arora et al.[12] conducted an experimental study on the performance of a solar flat-plate collector with Marquise-shaped channels using Al2O3/water nanofluid and pure water. The results demonstrated that the maximum energy efficiency achieved was 83.17% for nanofluids, significantly higher than the 59.72% for water using nanofluids and specialized absorber design in enhancing collector performance. Sheikholeslami et al [13] investigated the impact of aluminum oxide nanofluids and twisted tapes on heat transfer and energy efficiency in solar flat plate collectors. The results indicated that the combination of nanofluids and twisted tapes can significantly enhance performance, resulting in reduced exergy losses. Panda et al.[14] investigated the performance of a Flat Plate Solar Collector (FPSC) using water-CuO nanofluid, analyzing the effects of tilting angle and porous material properties. The numerical results revealed that increasing the tilting angle and curvature parameter enhanced the heat transfer rate, the porosity parameter effectively controlled it showed the potential for further heat transfer augmentation in solar collectors using nanofluids. Bezaatpour et al. [15] analyzed a novel design for flat plate solar collectors, incorporating rotary tubes and a magnetic field inducer to enhance the performance of Fe3O4/water nanofluid. The result showed that the combined approach increased the collector's energetic efficiency from 44.4% to 61.7% recovering approximately 300 W of lost energy with the magnetic inducer and rotary tubes individually restoring 27.8% and 10.44% of lost energy. Yan et al.[16] conducted a numerical analysis of a parabolic solar collector with a U-shaped absorber tube, using two-phase non-Newtonian nanofluids to optimize energy efficiency. The results showed that energy efficiency increased with Reynolds number reaching a maximum at Re = 5000, and that dual-pass pipes consistently showed single-pass pipes with the U-shaped design enhancing heat permeation due to reduced pipe diameter. Suthahar et al. [17] investigated the thermal and friction characteristics of a thermosyphon solar flat plate collector using Al2O3/water nanofluid with a helical twist insert. The results indicated that increasing the nanoparticle volume concentration enhanced the convective heat transfer coefficient and thermal performance but also led to higher pressure drop and friction with the modified collector showing superior heat removal compared to a conventional riser tube collector. Hussein et al.[18] studied the performance of a flat plate solar collector (FPSC) using hybrid nanofluids containing covalent functionalized multi-wall carbon nanotubes (CF-MWCNTs) and graphene nanoplatelets (CF-GNPs) with hexagonal boron nitride (h-BN) in distilled water. The results demonstrated that the thermal efficiency of the FPSC improved by up to 85% at a 4 L/min flow rate with increased nanoparticle concentration enhancing thermal energy gain and resulting in higher outlet temperatures. Peng et al. [19]conducted a three-dimensional numerical study of a U-shaped evacuated tube solar collector using various oxide nanofluids, including water–Al_2O_3, water–CuO, and water–TiO_2, under steady-state conditions. The results revealed that increasing the length and diameter of the U-shaped tubes significantly enhances thermal efficiency, with the water–CuO nanofluid achieving a 13.8% higher collector thermal efficiency compared to pure water along with improvements of 1.5% and 1.3% over water–TiO_2 and water-Al_2O_3, respectively. Eltaweel et al.[20] investigated the thermal performance enhancement of stationary flat-plate solar collectors by comparing the heat exchanger efficiency of normal circular tubes and twisted tubes. The results demonstrated that the twisted tube configuration improved performance by 12.8% and 12.5% when using distilled water and MWCNT/water nanofluid, respectively. It achieved a remarkable of 34% enhancement for twisted tubes with MWCNT compared to normal circular tubes with distilled water. Allouhi et al. [21] characterized the performance of a heat pipe flat plate solar collector utilizing nanofluids, employing a 1-dimensional transient heat transfer model to predict temperature variations. The study found that CuO-based nanofluid yielded the highest energetic and exergetic efficiency improvements at 2.7% and 11.1%, respectively, achieving a 2.95% increase in daily thermal energy generation compared to water, despite a maximum pressure drop increase of 13.26% at 3% nanoparticle loading. Munuswamy et al. [22] aimed to reduce greenhouse gas emissions by optimizing a solar flat plate collector with integrated rifled tubes and longitudinal fins to enhance thermal heat transfer. The study revealed that the use of CuO and Al_2O_3 nanoparticles at weight fractions of 0.2% and 0.4% significantly improved the thermal efficiency achieving enhancements of 2.1% to 5.5% for un finned and finned tube collectors, respectively with Al_2O_3 nanoparticles yielding efficiency increases of up to 7.8% compared to pure distilled water. Based on the above literature, the potential of nanofluids and various absorber designs in improving solar collector efficiency is clearly demonstrated even though the exploration in the field of nanofluids and solar collector has been extensive, the specialized studies on the effects of nanoparticle properties, shape of absorber tube with different strip design, and flow characteristics remain limited. The performance of conjugate shaped absorber tubes with zig zag rectangular angular strips of different nanofluids to maximize collector efficiency has not been extensively studied. Hence, this current study aims to experimentally investigate the performance of a flat plate solar collector using three different nanofluids with a zigzag rectangular shaped angled strip absorber design. This study also explores the use of various nanofluids, including MgO/DIW, ZnO/DIW, and Al2O3/DIW at a 1.0% volume concentration as the working fluid to determine their potential for enhancing the thermal efficiency of the solar collector. The selection of MgO, ZnO, and Al2O3 nanofluids for this study is based on their excellent thermal conductivity, stability, and compatibility with water-based systems. MgO offers high thermal conductivity and low density, reducing sedimentation in nanofluid suspensions. ZnO is chosen for its enhanced heat transfer properties and ability to improve both thermal and optical performance in solar systems. Al2O3 is widely researched due to its high chemical stability and reliable performance in improving heat transfer efficiency, making it an ideal candidate for solar thermal applications. The experiments were conducted with 45^0 angled strips at three different pitch ratios under identical working conditions. The performance of the rectangular shaped zigzag strip enhanced collectors was systematically compared to that of plain conjugate flat-plate solar collector collectors. The findings highlight the significant improvement in thermal efficiency and overall performance, emphasizing the potential of optimized angled strip designs and nanofluids in advancing solar energy systems. In addition to the use of nanofluids, the incorporation of heat transfer enhancement techniques such as the inclusion of angled strips inside the absorber tube has been investigated to improve the performance of solar thermal collectors. These modifications can promote increased fluid mixing and turbulence leading to improved heat transfer characteristics. The present study combines both approaches, exploring the performance of a conjugate flat-plate solar collector with the inclusion of zigzag rectangular shaped angled strips and the use of three different nanofluids as the working fluid.

2 Characteristics of nanofluids

High purity nanoparticles (MgO, ZnO and Al_2O_3) and DIW were procured from Sigma-Aldrich PVT LTD. SEM (Scanning Electron Microscope) imaging is to analyze and determine the morphological characteristics and elemental composition of the MgO, ZnO and Al_2O_3 nanoparticles. The morphology of the nanoparticles was precisely detailed in the Fig.1 (a-c) obtained from these reliable commercial sources. The SEM image of magnesium oxide nanoparticles reveals an irregular and highly porous structure. This morphology provides a large surface area-to-volume ratio making MgO nanoparticles highly effective in enhancing thermal properties when dispersed in a base fluid. The greater surface area results in more interaction with the fluid molecules, thereby improving heat transfer. In contrast, zinc oxide particles exhibit a closer-to-spherical shape with some irregularity. This shape is beneficial in balancing thermal conductivity and fluid stability, but due to fewer interaction points compared to MgO nanoparticles the thermal conductivity improvement is less pronounced. Al_2O_3 particles offers spherical shape that provides the least interaction with the base fluid resulting in a reduction in thermal conductivity compared to MgO nanoparticles. However, their symmetry leads to better suspension stability, making them ideal for long-term dispersion stability in applications where minimal agglomeration is crucial such as in coolant systems

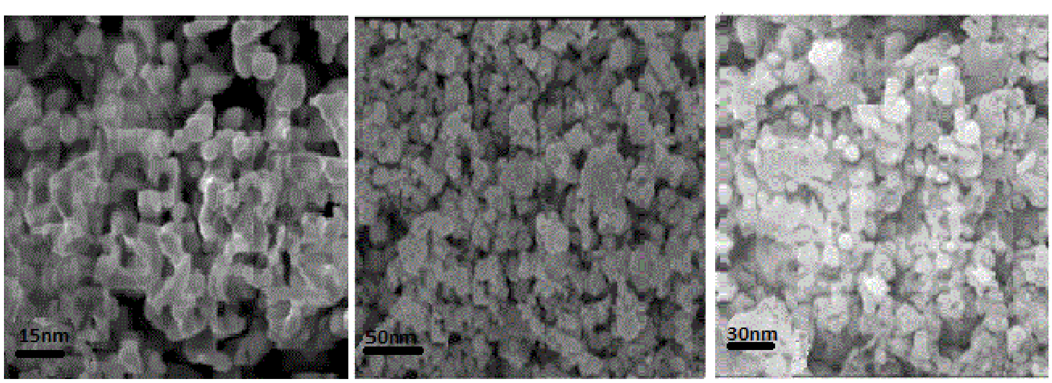

(a) (b) (c)

Fig. 1 The SEM images a) MgO Nanoparticles b)ZnO Nanoparticles c)Al_2O_3 Nanoparticles

3 Preparation of Nanofluids

Nanoparticles of ZnO, MgO, and Al_2O_3 were acquired from Sigma Aldrich Pvt Ltd and dispersed in deionized water to obtain a precise 1.0% volume concentration. The nanoparticles were weighed in a digital weight balance to achieve the desired 1.0% volume concentration. A two-step method was employed to prepare the high-performance nanofluids. Initially, the nanoparticles were dispersed in deionized water for 1 hour using a magnetic stirrer . Subsequently, the dispersed nanofluids were subjected to 2 hours of sonication at 24 kHz and 400W enhancing the overall quality and performance of the nanofluid samples. The prepared nanofluids were then evaluated for their thermal conductivity, viscosity, and stability to ensure suitability for further experimentation. The stability of nanofluids were ensured using the photo capturing methods that detailed in the Fig.2 . The MgO nanofluid appears homogeneously dispersed showing a slightly cloudy appearance. This indicates that the MgO nanoparticles were well distributed in the base fluid on the day 1. After 30 days, the nanofluid remains relatively stable with little noticeable phase separation. The consistent cloudy appearance suggests that most MgO particles were well dispersed. The small size and irregular morphology of MgO nanoparticles result in a higher surface charge leading to strong electrostatic repulsion between particles. This repulsion prevents aggregation and helps maintain a stable dispersion over the time. Additionally, the high surface area of MgO promotes interactions with the base fluid keeping the particles more stable. The Al_2O_3 nanofluid also appears homogeneously dispersed with a slightly milky appearance indicating initial good dispersion. However, after 30 days, there is a noticeable separation with the top part of the base fluid appearing clearer suggesting some sedimentation of Al_2O_3 nanoparticles. The particles have started to settle due to gravity. Al_2O_3 nanoparticles are spherical that reduces their surface area and results in lower electrostatic repulsion compared to MgO. This lower repulsion allows for faster aggregation and sedimentation over a period of time. The spherical shape of Al_2O_3 also reduces interactions with the fluid leading to quicker phase separation. Initially, the ZnO nanofluid shows good dispersion with a bright milky appearance indicating that the particles were suspended in the fluid. After 30 days, there was significant sedimentation in the ZnO nanofluid with the top portion of the fluid appearing much clearer indicating that most ZnO particles have settled out of suspension. ZnO nanoparticles being relatively larger than MgO have a higher tendency to settle due to gravitational forces. Additionally, ZnO exhibits weaker van der Waals forces compared to MgO resulting in reduced suspension stability. The aggregation of ZnO nanoparticles over a period of time accelerates sedimentation.

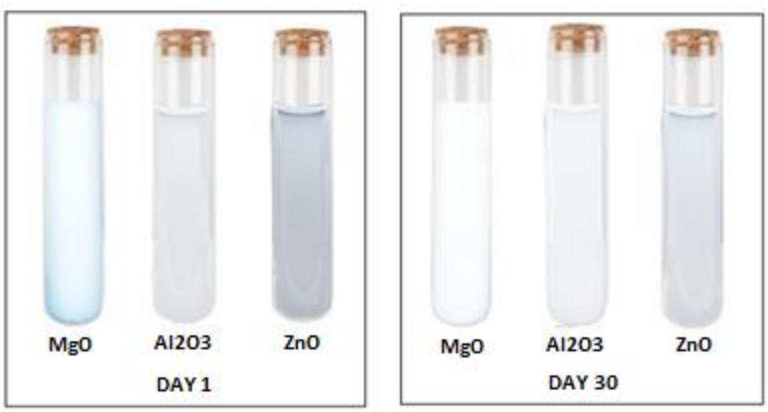

Fig. 2 Stability of nanofluids

4 Experimentation on test Rig

The experimental setup and instrumentation were detailed in Fig. 3. It includes a collector with an aperture area of 50 cm x 45 cm. The setup comprises copper tubes with a diameter of 20 mm and a length of 25 cm enclosed in a mild steel box measuring 66 cm × 50 cm × 25 cm. The mild steel box was painted black and insulated with glass wool. Rectangular shaped 45^0 angled strips are placed in a zigzag pattern over the rods inside the copper tubes. The corrugated copper tubes are covered by two glass plates. The mild steel box was tilted according to direction of sun. Six thermocouples were placed at various points including the inlet, outlet, and at top of glass plates. The flow rate is adjusted using a rotameter and control valve. Pressure gauges are installed at the entry and exit to measure the pressure difference. A heat exchanger is used to cool the working fluids at the outlet. The nanofluids are circulated through the test rig with the flow rate controlled by a valves using rotameter. The experimental setup allows the conjugated copper tubes and glass plates to be heated by sun radiation increasing transmittance and heating the copper tubes. The angled strips inside the tubes promote turbulence potentially enhancing heat transfer from the tube walls. The nanofluid temperatures were recorded at six locations using thermocouples. The heated nanofluids were then cooled in the heat exchanger and returned to the nanofluid tank. The experiments were repeated for three days to ensure the accuracy of the measurements

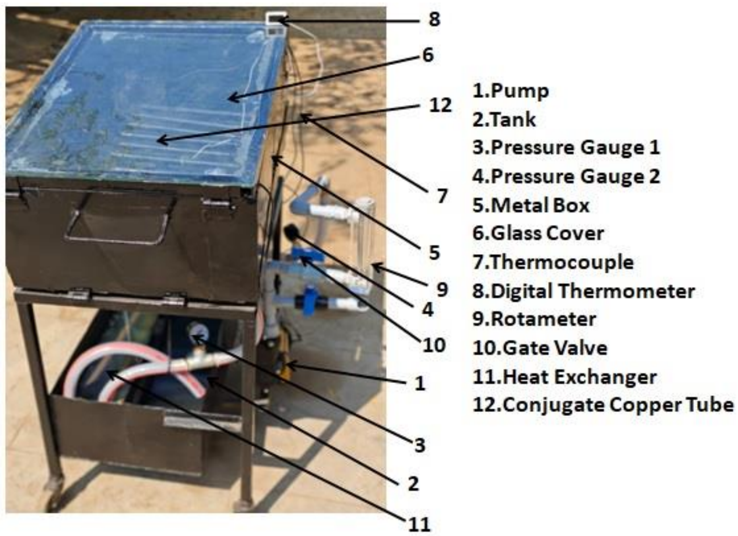

Fig. 3 Experimental Test Rig

5 Uncertainty Measurements

The uncertainty analysis for the experimental setup and measured parameters was conducted to assess the reliability and accuracy of the results. The details of the uncertainty analysis were provided in the following equations. The uncertainties of physical quantities like temperature, pressure, voltage, current, flow rate, length, and diameter impact the reliability of thermal characteristics such as the Heat transfer co efficient, Reynolds number, Nusselt number, Thermal efficiency, Friction factor and Pumping Power. The Holman method [23] was employed to evaluate the uncertainties for all experimental variables, as expressed in Equations Eq. 1 and 2, where the independent variables are represented as x1, x2, ..., xn and the corresponding absolute uncertainties are denoted as Wx1, Wx2, ..., Wxn. The calculated uncertainties for Heat transfer co efficient, Reynolds number, Nusselt number, thermal efficiency, friction factor and Pumping Power were found to be ±1.21%, ±2.21%, ±2.34%,±1.20%, ±1.85% and ±1.94% respectively.

$$W_R = \sqrt{\left(\frac{\partial R}{\partial x_1} Wx_1\right)^2 + \left(\frac{\partial R}{\partial x_2} Wx_2\right)^2 + \cdots + \left(\frac{\partial R}{\partial x_n} Wx_n\right)^2} \tag{1}$$

$$R = f(x_1, x_2, \ldots, x_n) \tag{2}$$

6 Model calculation

The heat transfer in the fluid is given by the equation Eq.(3)[24]

$$Q = mC_p(T_o - T_i) \tag{3}$$

Where, m is the Mass flow rate of the fluid, Cp is the Specific heat capacity of the fluid,

T_o is the outlet temperature of the fluid, T_i is the inlet temperature of the fluid

Heat Flux can be determined using the equation Eq.(4)

$$q = \frac{Q}{\pi d L} \tag{4}$$

Where, d is the Diameter of the tube and L is the length of the tube

The heat transfer co efficient is determined using the equation Eq.(5)

$$h = \frac{q}{(T_W - T_f)} \tag{5}$$

Where, T_w is the wall temperature and T_f is the fluid temperature

The Reynolds Number can be calculated using the equation Eq. (6) [25]

$$Re = \frac{\rho v D}{\mu} \tag{6}$$

Where, ρ is the Density of the fluid, v is the Velocity of the fluid,
D is the Diameter of the tube, μ is the Dynamic viscosity of the fluid

The Nusselt number can be calculated by using the equation Eq. (7) [26]

$$Nu = \frac{hD}{k} \tag{7}$$

Where, h is the Convective heat transfer coefficient, D is the Characteristic length or diameter of the tube , k is the Thermal conductivity of the fluid.

The Friction factor can be estimated using the equation Eq. (8) [27]

$$f = \frac{\Delta P}{\left(\frac{L}{d}\right)(\rho u^2)} \tag{8}$$

ΔP is the Pressure drop across the tube , L is the Length of the tube,
d is the Diameter of the tube , ρ is the Density of the fluid , u is the Fluid velocity.

The pumping power can be calculated by using the equation Eq. (9) [28]

$$Pp = \frac{\Delta P . V}{\eta_p} \tag{9}$$

Where, ΔP is the Pressure drop, V is the volumetric flow rate, η_p is the Pump efficiency

The thermal efficiency is determined using the equation Eq. (10) [29]

$$\eta = \frac{\dot{m}.C_p.(T_{out} - T_{in})}{A_c \, .G} \tag{10}$$

Where $\dot{m}$ is the Mass flow rate, Cp is the Specific heat capacity,
T_{out} is the Outlet temperature, T_{in} is the Inlet temperature , Ac is the Collector area ,
G is the Incident solar radiation or heat flux

7 Result and Discussion

7.1 The effect of heat transfer co efficient based on Reynolds number

Fig.4. shows the HTC variation of various nanofluids in PT and 45^0 angled zigzag rectangular strip configurations with different PRs across a range of Re. The results reveal the influence of PRs, nanoparticle type and Re on heat transfer enhancement. At a PRs of 2.0, the MgO/DIW, ZnO/DIW, and Al_2O_3/DIW exhibit significant improvements over DIW. At the higher Re, the HTC increased by 30%, 28% and 22% for MgO/DIW, ZnO/DIW and Al_2O_3/DIW, respectively. For a pitch ratio of 3.0 at the higher Reynolds number, MgO/DIW shows a 20% increase compared to ZnO/DIW and Al_2O_3/DIW. At the highest PRs of 4.0, MgO/DIW achieving a 15% improvement compared to DIW. This phenomenon was due to the addition of nanoparticles and the use of zigzag 45^0 angled rectangular strip with varying PRs significantly enhance the HTC compared to DIW [30]. The mechanisms behind the observed improvements include that nanoparticles increase the effective TC of the fluid thus enhancing the rate of heat transfer. Nanoparticles help in creating micro disturbances, reduces the thickness of the thermal boundary layer thereby increasing the convective heat transfer. As the pitch ratio increases, the HTC also increases. The zigzag arrangement of rectangular strips with higher pitch ratios induces more flow disturbances, improving turbulence and mixing that escalates higher HTR.

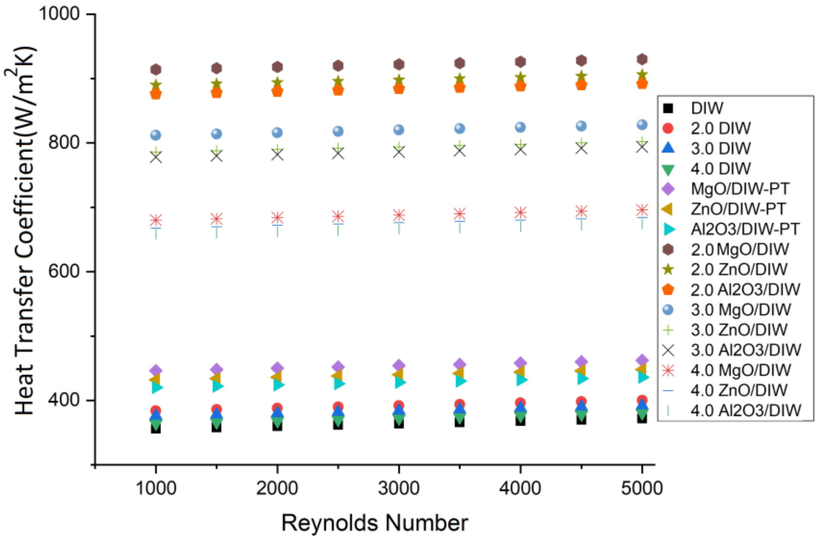

Fig.4. Effect of heat transfer coefficient based on Reynolds number

7.2 The effect of Nusselt number based on Reynolds number

Fig.5. illustrates the variation of the Nusselt number with Re for different nanofluids and PRs. For PRs of 2.0, the enhancement in the Nusselt number for MgO/DIW, ZnO/DIW, and Al_2O_3/DIW compared to the plain tube was observed as 45%, 42% and 40%, respectively. This significant increase can be attributed to the improved TC of the nanofluids and the greater turbulence intensity at higher Re. Tubes with smaller PRs of 2.0 showed a higher enhancement in the HTC than those with larger PRs of 3.0 and 4.0. This was due to the increased surface area available for heat transfer and the flow disruptions caused by the zigzag rectangular-shaped angled strips, induce secondary flows that improve turbulence. At a pitch ratio of 3.0, the Nusselt number increased by 32%, 30% and 28% for MgO/DIW, ZnO/DIW, and Al_2O_3/DIW compared to the plain tube. For a pitch ratio of 4.0, the improvements were slightly lower with increases of 24%, 22% and 20% for the corresponding nanofluids. This trend indicates that the utilization of nanofluid along with the geometries that promotes higher turbulence [31]. Among the nanofluids, MgO/DIW consistently showed the highest HTC across all Re and PRs owing to the higher TC of MgO nanoparticles. The ZnO/DIW and Al_2O_3/DIW nanofluids also showed substantial enhancements due to their own high thermal conductivities although slightly less effective compared to MgO/DIW Nanofluids. The use of zigzag rectangular-shaped angled strips and nanofluids in a solar flat plate collector system leading to synergistic effects on the enhancement in heat transfer.

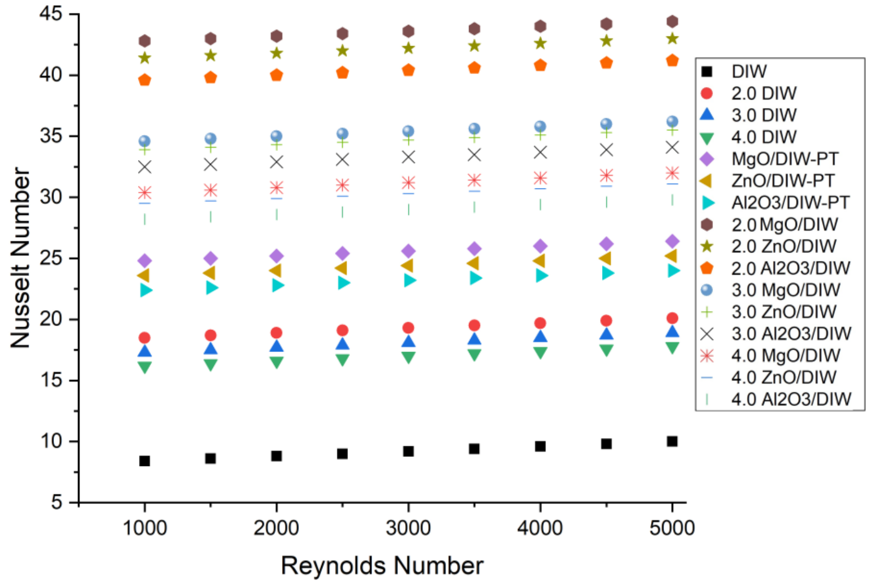

Fig.5 Effect of Nusselt number against Reynolds number

7.3 The effect of thermal efficiency based on Reynolds number

Fig.6. illustrates the relationship between TE and Re for various nanofluid compared to the baseline PT with DIW. The result reveals significant improvements in TE with the use of MgO/DIW, ZnO/DIW, Al_2O_3/DIW nanofluids and varying PRs of 2.0, 3.0, and 4.0. Among three nanofluids, MgO/DIW exhibits the highest TE across all PRs and Re. As the Re increases from 1000 to 5000, the TE shows a notable upward trend for all configurations, indicating improved convective heat transfer. At a Re of 5000, the thermal efficiency of nanofluids reaches around 85% against the PT with DIW achieves only about 45% due to more frequent flow disturbances that lead to higher turbulence levels over the PT at the same Re. For a PRs of 3.0, the efficiency increases are slightly lower around 65%, while for a PRs of 4.0, the improvements drop to 55%. The reduced efficiency for larger PRs was attributed to decreased flow disturbances resulting in relatively lower turbulence and less efficient heat transfer. This was due to the higher thermal conductivity and specific heat of MgO nanoparticles, facilitates better heat transfer enhance the energy transfer rate at the molecular level. At the molecular level, the addition of nanoparticles to DIW alters the thermal properties of the base fluid. Nanoparticles with high TC such as MgO and ZnO increase the TC of the nanofluid enabling more efficient heat transfer [32]. The suspended nanoparticles enhance energy transfer by promoting Brownian motion and micro-convection, disrupts the fluid layers near the tube wall thinning the thermal boundary layer. This phenomenon increases heat transfer from the fluid to the tube surface. The effect was more pronounced at higher Reynolds numbers due to the intensified turbulence that facilitates rapid molecular motion and energy transfer. The smaller PRs further increases this effect by frequently disturbing the flow and enhancing the mixing of nanoparticles within the fluid [33].

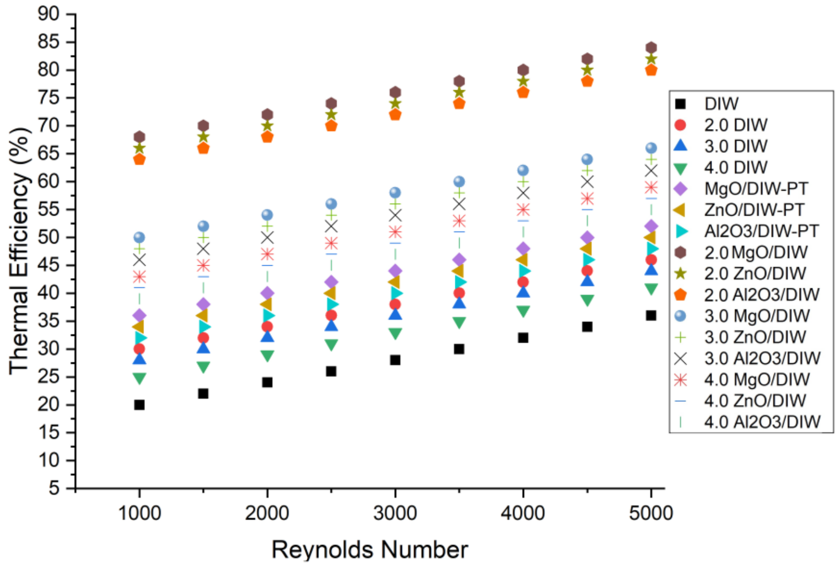

Fig.6 Effect of thermal efficiency against Reynolds number

7.4 The effect of friction factor based on Reynolds number

Fig.7 provided the FF as a function of Re for three different nanofluids in both PT and zigzag rectangular angled strip placed tubes with varying PRs such as 2.0, 3.0 and 4.0. The FF increases by 15 % for ZnO/DIW nanofluids at lower Re compared to DIW in zigzag rectangular strip angled tube. The FF decreases with increasing Re, a known behavior in fluid flow as the system transitions from laminar to turbulent flow regimes. ZnO/DIW nanofluids show higher FF compared to the DIW indicates enhanced interactions between the fluid and tube surface resulting in increased flow resistance. The FF for ZnO, MgO, and Al_2O_3 nanofluids was higher compared to DIW and the difference was more at lower Re. This shows that nanoparticles increase the viscosity of fluids and alter flow characteristics leading to more significant drag forces at lower flow rates. The interaction between nanoparticles and the tube wall at a molecular level plays a crucial role in this increased friction. Nanoparticles tend to accumulate near the tube wall due to shear-induced migration and Brownian motion. This migration creates a layer of denser fluid near the wall enhancing momentum transfer between the fluid and the tube resulting in a higher friction factor [34]. For all Re, the FF in zigzag rectangular strip tubes of higher pitch ratios like 2.0, 3.0, 4.0 is generally higher compared to PT. This is due to the enhanced surface roughness and secondary flow induced by the angled strips. The angled strips disturb the flow and increase turbulence intensity leading to higher friction losses. At the molecular level, the chaotic motion induced by the strips enhances the interaction between nanoparticles and the tube surface further increasing the FF. The FF increases as the PRs decreases from 4.0 to 2.0 indicating that closer spacing of the angled strips intensifies the turbulence and flow disturbances at lower Re. At lower Re, the zigzag structure causes localized eddies and flow separation, increases friction. As the pitch ratio decreases, these effects cause higher energy dissipation and FF. This increase diminishes slightly as the Re enhanced due to the dominance of inertial forces over viscous forces at higher flow rates.

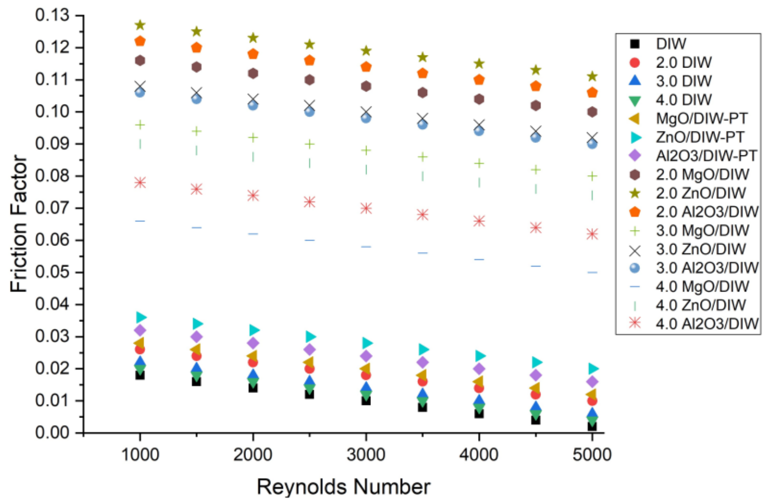

Fig.7 Effect of friction factor against Reynolds number

7.5 The effect of Pumping Power based on Reynolds number

Pumping power is a critical parameter in fluid flow systems especially when nanofluids are involved as it reflects the energy required to maintain the flow. Fig. 8 illustrates the relationship between PP and Re for different nanofluids in PT and zigzag rectangular angled strip placed tubes with various pitch ratios of 2.0, 3.0 and 4.0. ZnO/DIW nanofluids at 2.0 PRs showed higher PP by 10 % compared to the base fluid DIW at higher Re for Zigzag rectangular strip tubes compared to plain tubes. This increase was due to the higher viscosity of nanofluids and the enhanced interactions with the tube wall. The PP increases with increasing Re. The higher Re corresponds to higher flow rates requires more energy to overcome frictional resistance inside the tube. The addition of nanoparticles increases the effective viscosity of fluid thus requiring more energy to pump the fluid. Nanoparticles tend to migrate toward the tube walls due to shear forces creating a denser boundary layer near the wall increases the frictional losses and PP. The angled strips introduce flow disturbances and increase the turbulence intensity, higher frictional losses and energy requirements for pumping [35]. The presence of these strips increases secondary flow and disrupts the boundary layer near to the wall further increases the PP. In addition, the closer spacing of the angled strips intensifies the flow disturbances and increases flow resistance. At lower pitch ratios, the flow faces more frequent interruptions due to the proximity of the angled strips resulting in higher energy dissipation and thus requiring more PP to maintain the flow.

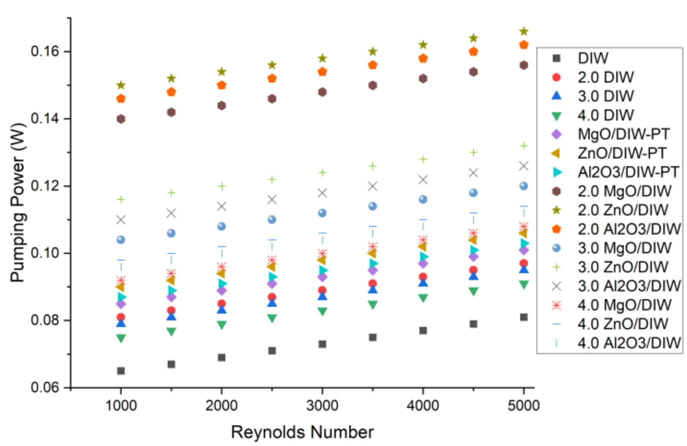

Fig.8 Effect of Pumping Power against Reynolds number

8 Conclusion

This study highlight the significance of the key findings derived from the comprehensive experimentation involving both plain tubes and zigzag rectangular-shaped angled strips in the conjugate solar flat plate collector with various nanofluids and distilled water. This provides the conclusion as follows

MgO/DIW nanofluid exhibited the highest HTC with an increase of 30% at a pitch ratio of 2.0 compared to DIW followed by 28% for ZnO/DIW) and 22% for Al_2O_3/DIW at higher Reynolds numbers.

The Nusselt number increased by 45%, 42% and 40% for MgO/DIW, ZnO/DIW, and Al_2O_3/DIW respectively for the pitch ratios of 2.0.

MgO/DIW achieved the highest thermal efficiency of 85% at higher Reynolds numbers, while the plain tube with DIW showed only 45% of efficiency. The thermal efficiency dropped to 65% and 55% for pitch ratios of 3.0 and 4.0, respectively.

ZnO/DIW nanofluid had a 15% higher friction factor at lower Reynolds numbers compared to DIW. The friction factor generally decreased with increasing Reynolds numbers.

The pumping power required for ZnO/DIW nanofluids at a pitch ratio of 2.0 was 10% higher compared to DIW due to the higher viscosity and increased frictional losses due to nanofluids.

These results revealed that the combination of zigzag strip configurations with MgO/DIW nanofluids provides the most effective thermal performance enhancements for potential applications in heat exchanger and solar energy systems.

Nomenclature

SFPC- Solar Flat Plate Collector	f-Friction Factor
CSFPC- Conjugate Solar Flat Plate Collector	TE-Thermal Efficiency (%)
TTI-Twisted Tape Insert	Cp- Specific heat (J/kgK)
PRs – Pitch Ratios	TC- Thermal Conductivity(W/mK)
NN- Nusselt Number	PP-Pumping Power(W)
FF- Friction Factor	T_o- Outlet temperature of the fluid (K)
HTR - Heat Transfer Rate	T_i - Inlet temperature of the fluid (K)
DIW- Deionized Water	L: Length of test Rig (m)
HTC – Heat transfer Co efficient	T_f -: Film Temperature (K)
Q- Heat transfer (W)	T_w-Wall Temperature (K)
PT- Plain tube	Y- pitch ratio
Re-Reynolds Number	d- Diameter of tube (mm)

Reference

1. Lee et al. Sun Tracking Systems: A Review. *Sensors,* no.9 (2009):3875-3890.
2. Shin et al. Investigation of Nanofluids for Solar Thermal Storage Applications. *Proceedings of the ASME 2009 3rd International Conference on Energy Sustainability collocated with the Heat Transfer and InterPACK09 Conferences*, no.19–23 (2009): 819-822.
3. Javadipour et al. Characterization of $Al_{12}Mg_{17}$ Nanofluid by Dynamic Light Scattering and Beam Displacement Methods. *Cornell University*, (2023): 2306.13766.

4. Yang et al .Thermal Stability and Performance Testing of Oil-based CuO Nanofluids for Solar Thermal Applications. *Multidisciplinary Digital Publishing Institute*, no. 13(4) (2020):876-876.
5. Hai et al. Energy and cost management of different mixing ratios and morphologies on mono and hybrid nanofluids in collector technologies. *Engineering Applications of Computational Fluid Mechanics Taylor & Francis*, no 17(1) (2023): 2164620.
6. Hawwash et al. Thermal Analysis of Flat Plate Solar Collector Using Different Nanofluids and Nanoparticles Percentages . *Institute of Electrical and Electronics Engineers*, No.9 (2021): 52053-52066.
7. Mostafizur et al.Thermodynamic Analysis of a Flat Plate Solar Collector with Different Hybrid Nanofluids as Working Medium-A Thermal Modelling Approach. *Multidisciplinary Digital Publishing Institute*. no. 8. (2023): 1320-1320.
8. Sheikholeslami et al . Recent progress on flat plate solar collectors and photovoltaic systems in the presence of nanofluid: A review. *Elsevier BV*, no. 293 (2021): 126119-126119
9. Singh et al. Energy and Exergy Analysis of a Rectangular-Shaped Mini-Channel Flat-Plate Solar Collector Using Tio2-Water and Cu-Water Nanofluids. *Science and Engineering Research Support Society*, no. 2 (2023):806-826.
10. Saffarian et al. Heat transfer enhancement in a flat plate solar collector with different flow path shapes using nanofluid . *Elsevier BV*, no.146 (2019): 2316-2329.
11. Peng et al. Investigation of energy performance in a U-shaped evacuated solar tube collector using oxide added nanoparticles through the emitter, absorber and transmittal environments via discrete ordinates radiation method. *Springer Science Business Media*, no. 4 (2019): 2623-2631.
12. Arora et al. Energy and Exergy Analysis of Marquise Shaped Channel Flat Plate Solar Collector Using Al_2O_3–Water Nanofluid and Water. *Journals of solar Engineering* , no. 4 (2019) :041008.
13. Sheikholeslami et al. Analyzing entropy and thermal behavior of nanomaterial through solar collector involving new tapes . *Elsevier BV*, no.123 (2021) :105190.
14. Panda et al. Nanofluid Based Pipe Flow Analysis in Absorber Pipe of Flat Plate Solar Collector: Effects of Inclination and Porosity. *American Scientific Publishers*. no. 2 (2023) :458-464.
15. Bezaatpour et al. Design and evaluation of flat plate solar collector equipped with nanofluid, rotary tube, and magnetic field inducer in a cold region. *Elsevier BV*, no. 170 (2021): 574-586.
16. Yan et al. Effect of U-shaped absorber tube on thermal-hydraulic performance and efficiency of two-fluid parabolic solar collector containing two-phase hybrid non-Newtonian nanofluids. *Elsevier BV*, no 185 (2020) :105832.
17. Suthahar et al .Experimental investigation on solar flat plate collector using alumina nanofluid with tube inserts. *Maney Publishing*, no. 3 (2020) 179-189.
18. Hussein et al. Thermal performance enhancement of a flat plate solar collector using hybrid nanofluid. *Elsevier BV*, no. 204 (2020) 208-222.
19. Peng et al. Investigation of energy performance in a U-shaped evacuated solar tube collector using oxide added nanoparticles through the emitter, absorber and transmittal environments via discrete ordinates radiation method. *J Therm Anal Calorim*, no.139 (2019) 2623–2631.
20. Eltaweel et al. Indirect thermosiphon flat- plate solar collector performance based on twisted tube design heat exchanger filled with nanofluid. *International Journal of Energy Research*, no.44 (2020) 4269 - 4278.
21. Allouhi et al. Heat pipe flat plate solar collectors operating with nanofluids. *Solar Energy Materials and Solar Cells*, no. 219. (2021)110798.
22. Munuswamy et al. Experimental investigation on lowering the environmental hazards and improving the performance patterns of solar flat plate collectors by employing the internal longitudinal fins and nano additives. *Environmental Science and Pollution Research*, no.27. (2020) 45390–45404.
23. Holman et al. Experimental Methods for Engineers. *seventh ed. McGraw-Hill, New York*, (2001).
24. Shajahan et al .Heat transfer investigations of in-line conical strip inserts using MWCNT/water nanofluid under laminar flow condition. *International Journal of Thermal Sciences*, no. 183(2023):107844.
25. Mwesigye et al. Heat Transfer and Thermodynamic Performance of a Parabolic Trough Receiver with Centrally Placed Perforated Plate Inserts. *Appl. Energy* ,no.136 (2014) :989-1003

26. Chaurasia et al. Numerical and Experimental Thermal Performance with Entropy Generation Analysis on Tube with Helical Screw Tape Inserts at Number of Strips in Turbulent Flow. *Proc. Inst. Mech. Eng. Part C J. Mech. Eng. Sci*. no. 235 (2021):1057–1070.
27. Chakraborty et al. Impact of Helical Coil Insert in the Absorber Tube of Parabolic Trough Collector. *Smart Innov. Syst. Technol*, no 206 (2021): 177–187.
28. Chakraborty et al. Heat Transfer Enhancement Analysis of Parabolic Trough Collector with Straight and Helical Absorber Tube. *Therm. Sci. Eng. Prog*, no.20 (2020) :100718.
29. Kalogirou et al. Solar Energy Engineering: Processes and Systems. *2nd ed.; Elsevier Inc.: Amsterdam, The Netherlands*, (2009).
30. Mebarek-Oudina et al . Entropy and convection effect on magnetized hybrid nano-liquid flow inside a trapezoidal cavity with zigzagged wall. *International Communications in Heat and Mass Transfer*, no.125 (2021):105279.
31. Bisheh et al. Impact of hybrid nanofluids (Ag- TiO2/H2O) on improving the performance of a heat exchanger with turbulent induction elements. *Engineering Reports*, no. 4 (2022):12502.
32. Louis et al. Application of Nanofluids in Improving the Performance of Double-Pipe Heat Exchangers-A Critical Review. *Materials*, 15 (2022): 6879.
33. Abdullah et al. Impact of coil pitch on heat transfer enhancement of a turbulent flow of α-Al_2O_3/DW nanofluid through helical coils. *Thermal Science*, no. 6 (2023):5005-5014.
34. Kwak et al. Numerical investigation of nanoparticle deposition location and pattern on a sharp-bent tube wall. *International Journal of Heat and Mass Transfer*, no.164 (2021):120534.
35. Huang et al. Energy dissipation mechanism of a centrifugal pump with entropy generation theory. *AIP Advances*, no.11 (2021):045208.

Submitted: 09.07.2024.
Revised: 28.10.2024.
Accepted: 04.12.2024.